AD-A119 986 SCHOOL OF AEROSPACE MEDICINE BROOKS AFB TX F/G 6/16
INTERFERENCE FRINGES USED TO DETERMINE RETINAL GANGLION CELL RE--ETC(U)
JUL 82 C M WORMINGTON
UNCLASSIFIED SAM-TR-82-23 NL

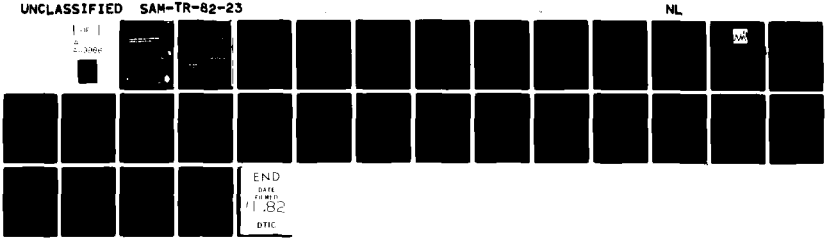

END
DATE FILMED
11-82
DTIC

Report SAM-TR-82-23

INTERFERENCE FRINGES USED TO DETERMINE RETINAL GANGLION CELL RECEPTIVE FIELD SIZES

Charles M. Wormington, Captain, USAF, BSC

July 1982

Final Report for Period September 1978 — March 1982

USAF SCHOOL OF AEROSPACE MEDICINE
Aerospace Medical Division (AFSC)
Brooks Air Force Base, Texas 78235

NOTICES

This final report was submitted by personnel of the Laser Effects Branch, Radiation Sciences Division, USAF School of Aerospace Medicine, Aerospace Medical Division, AFSC, Brooks Air Force Base, Texas, under job order [illegible].

When U.S. Government drawings, specifications, or other data are used for any purpose other than in connection with a definitely Government-related procurement, the United States Government incurs no responsibility or any obligation whatsoever. The fact that the Government may have formulated or in any way supplied the said drawings, specifications, or other data, is not to be regarded by implication, or otherwise in any manner construed, as licensing the holder, or any other person or corporation; or as conveying any rights or permission to manufacture, use, or sell any patented invention that may in any way be related thereto.

The animals involved in this study were procured, maintained, and used in accordance with the Animal Welfare Act of 1970 and the "Guide for the Care and Use of Laboratory Animals" prepared by the Institute of Laboratory Animal Resources - National Research Council.

The Office of Public Affairs has reviewed this report, and it is releasable to the National Technical Information Service, where it will be available to the general public, including foreign nationals.

This technical report has been reviewed and is approved for publication.

Charles M. Wormington

CHARLES M. WORMINGTON
Captain, USAF, BSC
Project Scientist

Charles H. Bonney

CHARLES H. BONNEY
Lieutenant Colonel, USAF, BSC
Supervisor

Roy L. DeHart

ROY L. DEHART
Colonel, USAF, MC
Commander

UNCLASSIFIED

SECURITY CLASSIFICATION OF THIS PAGE *(When Data Entered)*

REPORT DOCUMENTATION PAGE		READ INSTRUCTIONS BEFORE COMPLETING FORM
1. REPORT NUMBER SAM-TR-82-23	2. GOVT ACCESSION NO. AD-A117986	3. RECIPIENT'S CATALOG NUMBER
4. TITLE *(and Subtitle)* INTERFERENCE FRINGES USED TO DETERMINE RETINAL GANGLION CELL RECEPTIVE FIELD SIZES		5. TYPE OF REPORT & PERIOD COVERED Final Report Sep 1978 - Mar 1982 6. PERFORMING ORG. REPORT NUMBER
7. AUTHOR(s) Charles M. Wormington, Captain, USAF, BSC		8. CONTRACT OR GRANT NUMBER(s)
9. PERFORMING ORGANIZATION NAME AND ADDRESS USAF School of Aerospace Medicine (RZL) Aerospace Medical Division (AFSC) Brooks Air Force Base, Texas 78235		10. PROGRAM ELEMENT, PROJECT, TASK AREA & WORK UNIT NUMBERS 62202F 7757-02-53
11. CONTROLLING OFFICE NAME AND ADDRESS USAF School of Aerospace Medicine (RZL) Aerospace Medical Division (AFSC) Brooks Air Force Base, Texas 78235		12. REPORT DATE July 1982 13. NUMBER OF PAGES 27
14. MONITORING AGENCY NAME & ADDRESS *(if different from Controlling Office)*		15. SECURITY CLASS. *(of this report)* Unclassified 15a. DECLASSIFICATION/DOWNGRADING SCHEDULE

16. DISTRIBUTION STATEMENT *(of this Report)*

Approved for public release; distribution unlimited.

17. DISTRIBUTION STATEMENT *(of the abstract entered in Block 20, if different from Report)*

18. SUPPLEMENTARY NOTES

19. KEY WORDS *(Continue on reverse side if necessary and identify by block number)*

Electrophysiology	Monkey
Eye	Receptive field
Ganglion cell	Retina
Interference fringe	Spatial frequency

20. ABSTRACT *(Continue on reverse side if necessary and identify by block number)*

A method is presented for determining the effective diameter of retinal ganglion cell receptive field centers. Unaffected by the optics of the eye, the method involves single-unit recording of ganglion cell activity in response to drifting interference fringe patterns of various spatial frequencies. The ganglion cell response magnitude (contrast) falls off as the spatial frequency of the fringes is increased. From the spatial frequency dependence of the observed responses, the receptive field centers of the sampled X-cells were

DD FORM 1 JAN 73 1473 EDITION OF 1 NOV 65 IS OBSOLETE

UNCLASSIFIED

SECURITY CLASSIFICATION OF THIS PAGE *(When Data Entered)*

20. ABSTRACT (Continued)

estimated to range from 6.8 to 10 μm in diameter. Suggested improvements in the technique are discussed.

CONTENTS

INTERFERENCE FRINGES USED TO DETERMINE RETINAL GANGLION CELL RECEPTIVE FIELD SIZES

INTRODUCTION

To accurately predict ocular damage thresholds and safe exposure levels for lasers, we must know how the laser beam is distributed on the retina. One way of measuring this retinal point-spread function is to use the receptive field (RF) of a retinal ganglion cell as a microprobe light detector and to scan the laser image across the RF (23). In the Macaca mulatta (rhesus) monkey, the sustained color-opponent ganglion cells in the foveal area have the smallest RF centers, encompassing only a few cones at the most and probably only one (7). In other words, the microprobe light detector in this case could be a single-cone photoreceptor. The "detector output" is sampled at the ganglion cell level by extracellular recording methods.

To measure the retinal point-spread function using this technique, we must first determine the effective RF center diameter. The point-spread measurements can then be corrected for the finite probe size.

Many investigators have measured RF centers in intact eyes (13). In all cases, however, these measurements included distortion due to the optics of the eye. To circumvent this problem, we devised a new technique that involves forming an interference fringe pattern directly on the retina. This technique creates a retinal illumination pattern that is reportedly unaffected by aberrations or defocusing of the optical system of the eye (4,5,22).

The present investigation is directed, therefore, toward developing a method to determine the effective diameter of ganglion cell RF centers without distortion by optics of the eye. This method involves combining the interference fringe technique with single-unit recording of ganglion cell activity in the rhesus monkey.

EXPERIMENTAL METHODS

Extracellular recordings from retinal ganglion cells were made in rhesus monkeys.

Anesthesia

Initially, ketamine hydrochloride (Vetalar, 5-10 mg/kg) was administered intramuscularly to restrain the monkey. Sodium pentobarbital (Nembutal, 20-25 mg/kg, I.V.) provided surgical-plane anesthesia for the initial surgical procedures. Throughout the rest of the experiment, light anesthesia was maintained by continuous infusion of pentobarbital (3-5 mg/kg/hr, I.V.) in 5% dextrose, lactated Ringer's solution (4-6 ml/hr). A local anesthetic (2% lidocaine jelly) was applied at all incision margins and pressure points.

Since the experiments required a minimum of eye movement, gallamine triethiodide (Flaxedil, 5-10 mg/kg, I.V.) was injected every 30 minutes. The neuromuscular blockade was interrupted at the end of a recording session and was resumed the following day.

To avoid cumulative effects of fixed infusion levels of anesthetic over the three days of the experiment, dosages were adjusted to satisfy the following criteria: (a) tachycardia and transient hypertension in response to strong noxious stimuli, and (b) stage I or transition between stage I and II electroencephalogram (EEG) waveforms.

Physiological Monitoring

A tracheotomy was performed, and the animal was respired artificially with a ventilator (20 strokes/min, 25-45 cc/stroke). Expired pCO_2 (4-5%) was monitored continuously with a Beckman Model LB-2 medical gas analyzer. The pCO_2 level was adjusted by changing the stroke volume. Rectal temperature was monitored with a thermistor and maintained at 37° ± 1°C with the aid of a thermal blanket. The electrocardiogram (Lead II), EEG (leads on posterior temporal and occipital areas), urine output, and mean arterial blood pressure were also continuously monitored.

Stimulus Systems

Incoherent Light Source--Light stimuli were obtained from a 150-watt xenon arc lamp (color temperature ca. 6000°K) with two independent light beams presented to the eye in Maxwellian view (see Fig. 1). The wavelength of the test beam was varied by narrow-band interference filters (420-640 nm in 20-nm increments) with bandwidths at half-maximum of 10 ± 2 nm and a peak transmission of 42% or more. The interference filters were checked for side bands in a spectrophotometer and calibrated with an EG&G Model 580 radiometer. The energy of the test beam was varied with neutral density filters that had been calibrated in a spectrophotometer and in the optical system with the radiometer. Apertures mounted on a rotatable wheel provided circular stimuli that were projected onto the retina.

A second beam projected an adapting background light of 20° diameter onto the retina. This beam was presented through a fiber-optic cable and modified fundus camera. White light was used as a neutral background. Colored backgrounds were obtained by broadband filters with sharp cutoff (Rolyn Optics, 66.1060 (red, 590-700 nm), 66.1055 (green, 480-580 nm), and 66.1050 (blue, 350-490 nm)). These filters were calibrated in a spectrophotometer and in the optical system with a radiometer and inserted narrow-band interference filters. Calibrated neutral density filters modified the intensity of the beam.

Interference-fringe Generator--Sinusoidal interference fringes were generated on the retina by a modified version of the Thomas Young double-pinhole technique. The technique used in this study is essentially like that developed by Westheimer (22).

A krypton laser ($Laser_1$; Spectra Physics Model 170, 530-nm line) provided the coherent light source. A beam telescope (BT; Tropel Model 280 laser

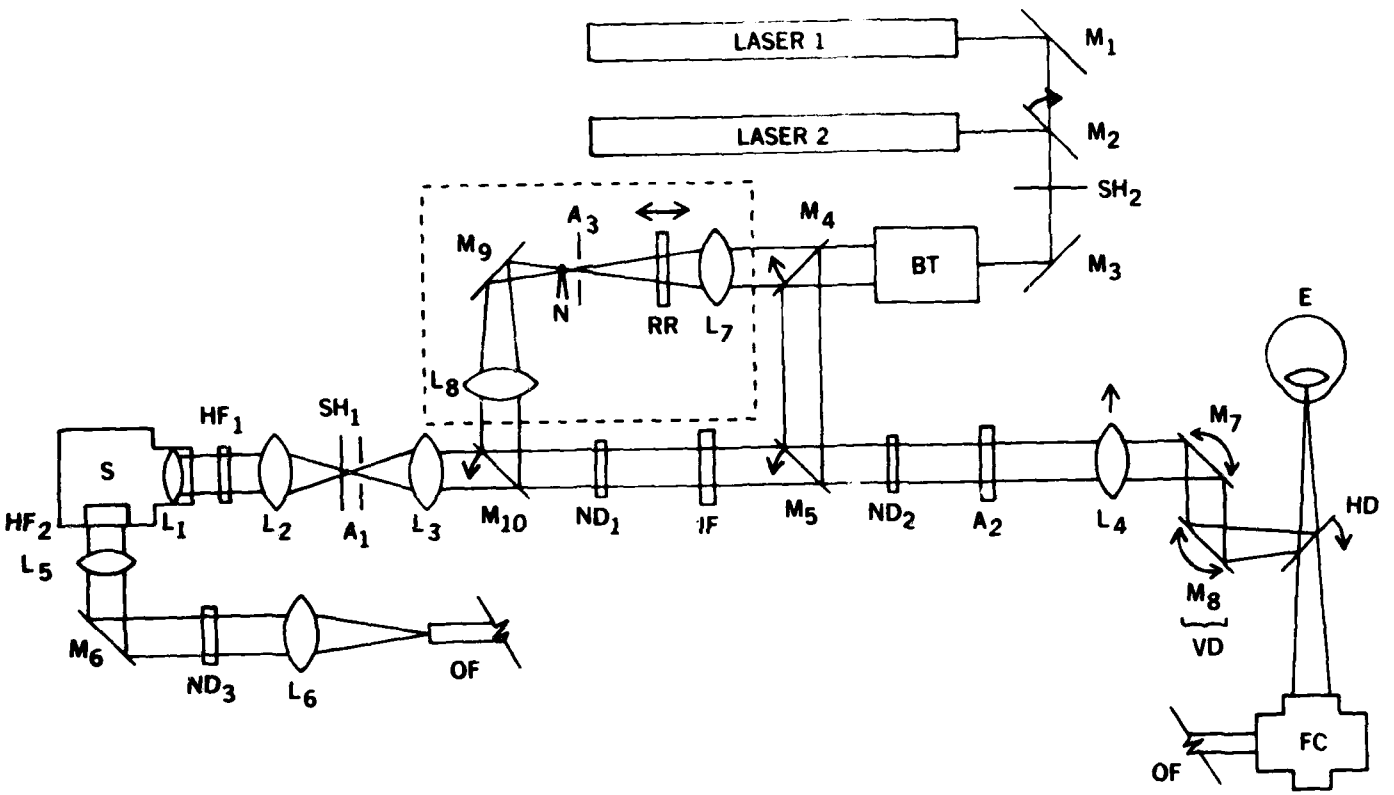

Figure 1. Schematic diagram of optical system. Laser$_1$, krypton laser (647 nm); laser$_2$, krypton laser (530 nm); S, xenon arc lamp; L_1, L_3, L_5, collimating lenses; HF_1, HF_2, heat filters; L_2, L_6, condensing lenses; SH_1, SH_2, electromagnetic shutters; A_1, aperture; ND_1, ND_2, ND_3, neutral density filter trays; IF, interference filter tray; M_1, M_3, M_6, front-surface mirrors; M_2, M_4, M_5, M_7, M_8, M_{10}, movable front-surface mirrors; A_2, aperture wheel; L_4, removable Maxwellian lens; VD, vertical deflector (shown horizontal, but actually M_8 is mounted vertically over M_7); HD, horizontal deflector (movable glass plate); E, eye; BT, beam telescope; OF, optic fiber (to flash optical system of FC); FC, fundus camera. The interference fringe generator is shown within the dashed rectangle: L_7, converging achromat; RR, movable Ronchi ruling; A_3, iris diaphragm; N, thin tapered metal needle; M_9, front-surfaced mirror; L_8, collimating achromat.

collimator and Model 261 spatial filter) expanded the laser beam to a diameter of 50 mm. This collimated beam passed through an achromatic lens (L_7; focal length of 34 cm) and a Ronchi ruling (RR; 300 lines per inch). The Ronchi ruling broke the beam into a series of diffraction spots that were focused by L_7 onto an iris diaphragm (A_3). The diaphragm occluded all diffraction spots of second order and greater. A small tapered needle (N) positioned at the center of the diaphragm aperture occluded the zero-order diffraction spot. Hence this spatial filter occluded all but the two first-order spots. These two spots of equal intensity were then imaged at the nodal point of the animal's eye by two achromats (60-cm (L_8) and 18-cm (L_4) focal lengths). Where the two laser beams overlap on the retina, an interference fringe pattern is formed. The spatial frequency of this pattern varies inversely with the distance between the two images in the nodal plane. To vary this distance, the spacing between the Ronchi ruling and L_7 was varied. The spatial filter (A_3 + N) was then adjusted to pass only the first-order images. A telemicroscope was used to monitor and set the spatial filter.

The interference pattern formed on the retina is essentially independent of the optics of the eye (4,5,22). The intensity distribution of the interference pattern is given by:

$$I(x) = I_1 + I_2 + 2\sqrt{I_1 I_2}\cos\left(\frac{2\pi d \sin\alpha}{\lambda}\right)$$

where

I_1, I_2 = intensities of the two beams

d = separation of the two coherent sources at the nodal point of the eye

α = angular distance in radians along the retina

λ = wavelength of the coherent light

When the two beams are of equal intensity, the fringes are of unity contrast. Because of the possible scattering of the beams within the eye, the assumption of unity contrast at the level of the retina is somewhat idealized. The actual distribution, however, is not likely to differ from this by more than a few percent (22).

The pattern on the retina was rectangular (3° x 5°) with the fringes oriented horizontally. The spatial frequency for various positions of the Ronchi ruling was calibrated before each experiment.

To evaluate the quality of our interference fringe patterns and to model the ganglion cell, we used an apertured photomultiplier (PM) tube as a light probe. The two first-order spots were imaged as in an experiment, except no eye was present. The PM tube was located 492 cm from the focus point of the two spots. A 400-μm pinhole aperture was placed in front of the PM tube to model the effective RF center of a ganglion cell. This aperture subtended a visual angle of 0.28 minute of arc. On the rhesus retina this angle would correspond to a 1.2-μm-diameter RF center.

The output of the PM tube was connected to a voltage-controlled oscillator (VCO; Wavetek Model 116) and to a storage oscilloscope. As the light

intensity hitting the PM tube varied, the frequency of the VCO sine wave output varied. This modelled the ganglion cell output. The VCO output was then processed through the pulse height discriminator and the computer to give averaged histograms.

In Figure 2, A shows an example of the direct PM-tube voltage output for drifting interference fringes with a spatial frequency of 11.6 cycles/degree; B shows the histogram of the pulse-height discriminator output for the same conditions as in A; and C shows the "filtered" histogram of the pulse-height discriminator output. The peak-to-peak amplitude in each of these examples varies by a factor of about 1.7.

Figure 3 shows more examples of filtered, processed PM-tube outputs for a 0.28' aperture. The spatial frequency of the interference fringes in A is 22.4 cycles/degree; in B, 11.6 cycles/degree. The only other difference between A and B is that B was sampled for 0.56 second longer than A. The peak-to-peak amplitude varies by a factor of about 1.8 in these examples. Hence these examples show that the interference fringe patterns in our experiments are not perfect sinusoids and vary in peak-to-peak amplitude.

Laser Spot Sources--The krypton laser (530 nm) used for the interference fringe generation and another krypton laser ($Laser_2$; 647-nm line) were also used to project minimal spots onto the retina. These spots were used to center the beam on the RF center. Calibrated neutral density filters modified the intensity of the laser image. Since both beams were expanded by the beam telescope to a 50-mm diameter and since the pupil was about 8 mm in diameter, the distribution of the beam that entered the eye was essentially uniform. The beam intensity at the corneal plane was measured with a radiometer (EG&G, Model 580). During the experiments the beam was continuously monitored with a photodiode.

Both the laser beam and the xenon beam were presented to the eye via a glass-plate deflector mounted between the fundus camera and the eye. The deflector and a system of two mirrors displaced the beam on the retina by deflecting the beam about the horizontal and vertical axes through the nodal point of the eye. The deflector system was driven by two hydraulic microdrives (David Kopf Inc, Model 607W with electronic control and display), controlled either manually or by a PDP 11/03 computer (25).

Electrophysiological Recording

Borosilicate glass capillaries with inner filaments were used to make microelectrodes (10-35 MΩ impedance in situ). They were pulled on a vertical puller and then filled with 3M potassium acetate. The reference electrode was a stainless-steel needle in the vitreous humor. During the experiment, a Faraday cage surrounded the animal. The ganglion cell activity was recorded extracellularly by a negative capacitance electrometer amplifier (Stoelting, Model P1) and an AC-coupled amplifier, displayed on a storage oscilloscope, stored on magnetic tape, and made audible via an audio monitor.

The stimulus, beam deflection, and recording systems interfaced with a PDP 11/03 computer (25). The amplified signal was filtered by 10-kHz hi-pass and 1-kHz lo-pass filters. A window discriminator (W-P Inst. Inc, Model 120)

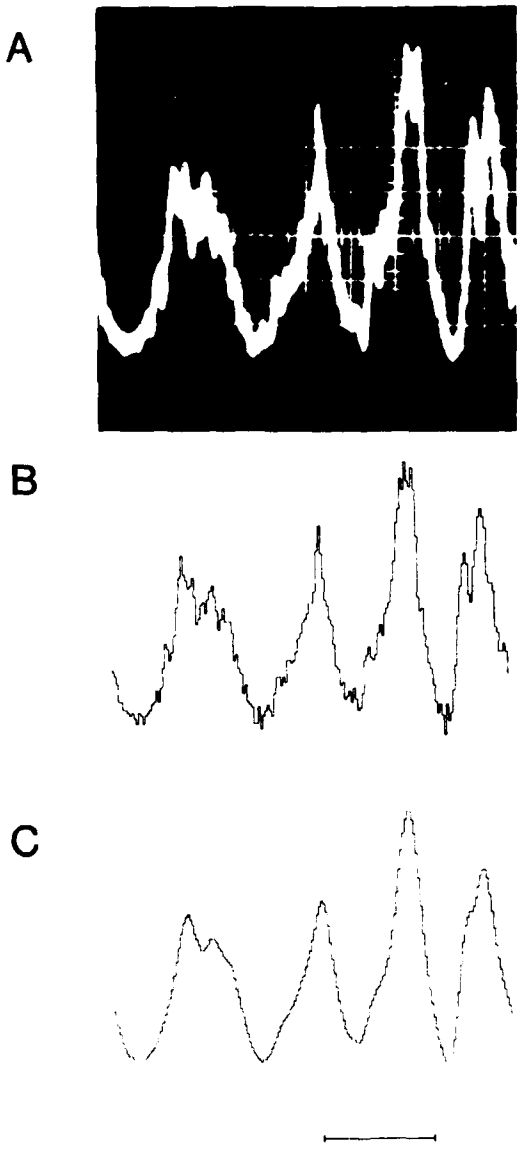

Figure 2. Photomultiplier (PM) tube output and histograms of pulse-height discriminator output for 530-nm interference fringes moving in one direction. A: Photograph of oscilloscope trace of PM-tube voltage output. The PM-tube aperture was a 400-μm pinhole (0.28 min of arc). Interference fringes that drifted across the aperture had a drift frequency of 2.7 Hz and a spatial frequency of 11.6 cycles/degree. B: Histogram of PM-tube output that has been processed through a voltage-controlled oscillator, a pulse-height discriminator, and a computer. Average of 30 sweeps in same direction, 10 msec/bin. C: Filtered histogram of processed PM-tube output. Calibration bar: 500 msec.

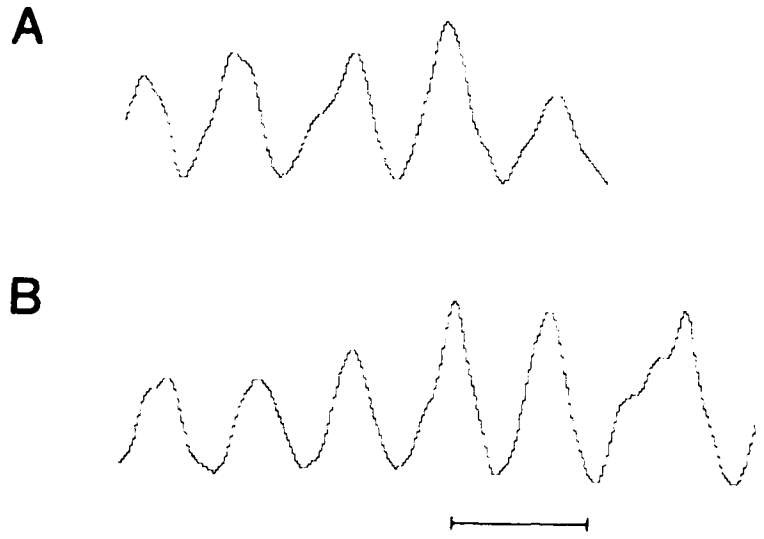

Figure 3. Examples of interference fringe patterns. Both graphs are histograms of the processed PM-tube output. Average of 30 sweeps across a 400-μm aperture (0.28') with a drift frequency of 2.7 Hz. A: 22.4 cycles/degree. B: 11.6 cycles/degree. Calibration bar: 500 msec.

was used to generate a 200-μsec, 5-volt rectangular pulse for each action potential. These pulses were then counted by the computer, and the number of pulses in each 10-msec bin was stored on a magnetic disk. Average response histograms were plotted on a graphics CRT terminal on-line.

Stabilization of Retinal Tissue

Retinal movements must be minimized before small images can be measured. Mechanical disturbances were minimized by mounting the preparation, preamplifier, lasers, and optical systems on a heavy Newport pneumatic isolation table. The extraocular muscles were paralyzed with gallamine triethiodide (Flaxedil, 10-20 mg/kg/hr, I.V.) (18). Respiratory and pulse movements of the retina were minimized by severing the trachea above the cannulation, maintaining near-normal intraocular pressure, bilateral cervical sympathectomy, cutting the carotid sheath and adjacent connective tissue, and ipsilateral pneumothorax. Retinal movements were monitored by the mechanoelectric transducer action of the micropipette electrode as well as by observation of receptive field displacements with time.

Procedure

Mydriasis and cycloplegia were obtained by a combination of cyclopentolate hydrochloride (0.2%) and phenylephrine hydrochloride (1%) (Cyclomydril) instilled each 8 hours. The animal was placed on a platform (5 degrees of

freedom of movement) and positioned in a head-holder so that the fovea of the left eye could be seen in the center of the field of view of the fundus camera. Either a suture was placed through the eyelid to keep the eyelid open or the eyelid was cut away. At the beginning of the experiment, a contact lens was used to protect the cornea. (After the microelectrode was inserted into the vitreous, the contact lens was removed and a continuous corneal drip system was set up.) A canthotomy was then performed on the test eye and the conjunctiva was cut. A #64 Beaver blade was used to make a small vertical incision in the sclera (at the pars plana) down to the uvea; then a razor-blade knife was used to make a hole into the vitreous. The 16-gauge needle of a special closed-chamber system (24) was inserted into the hole, making a tight fit, and was left in place to serve as a guide for the microelectrode. This special closed-chamber system served to minimize vitreal leakage, to anchor the eyeball, and to provide a port for an isotonic saline column to maintain a constant intraocular pressure. The closed-chamber system was mounted on a special microelectrode positioner (24) that allowed fine mechanical movement of the microelectrode and guide needle. The electrode could be advanced into the eye and moved along vertical and horizontal axes on the retina; the scleral insertion point of the electrode was the center of rotation.

The microelectrode was inserted through the guide needle and driven slowly back to the retina with a hydraulic microdrive. Viewing through the fundus camera, the investigator positioned the electrode near the center of the fovea and then positioned the stimulus spot on the fovea. The retina was stimulated every second with a 200-msec pulse of 580-nm light. The stimulus frequency and pulse width were controlled by the computer through a shutter driver (Vincent Associates, Uniblitz Model 300B).

After a ganglion cell was found, the approximate center of its receptive field was determined by moving the stimulus spot on the retina until the strongest response was evoked. Then the cell was studied with different stimuli to characterize the cell. On-cells with sustained color-opponent responses and concentrically organized receptive fields were sought. Once the cell was characterized, the laser was used to form the interference fringe pattern on the retina. Some cells were studied in the presence of an incoherent adapting light of wavelength appropriate to suppress selectively the antagonistic surround mechanism. Hence, by using fringes of wavelength specific for the center mechanism, the receptive field center could be evaluated in isolation. By deflecting the laser beams along the vertical axis around the nodal point of the eye, the interference pattern was moved up and down on the retina, i.e., in a direction perpendicular to the fringes.

As fringe spacing was changed, the temporal (drift) frequency of the fringes across the receptive fields was kept constant by keeping the drift velocity inversely proportional to the spatial frequency of the fringes. The drift velocity was about 2.7 cycles/sec. That sustained ganglion cells of the rhesus respond to slowly moving sinusoidal grating patterns, modulating their responses around the spontaneous firing rate of the cell, has been shown (20).

After in vivo point-spread functions were measured, the beam deflection apparatus was calibrated. With the laser used during the experiment, lesions were placed on the retina at known intervals. After the animal was euthanized by injection of Barb-euthol (ca. 0.5 cc/kg, I.V.), the intact eye was enucleated, the globe was opened, and a rectangle (about 5 mm x 10 mm) of ocular

fundus was removed, including the area where the calibration lesions were placed. The fundus strip was then fixed in 4% glutaraldehyde and mounted beneath a cover glass with glycerin jelly. Rasmussen has shown that specimen shrinkage due to fixation under these conditions could be neglected (17). Finally, the fundus strip was examined under a light microscope at 35 or 100 power, and the distances between the centers of the calibration lesions were measured.

Determination of Receptive Field Center Diameter

The overlap of two coherent laser beams on the retina results in a spatial sinusoidal oscillation of electric field across the retina. By sweeping this spatial pattern across the RF center (e.g., a single cone) and monitoring the ganglion cell response as a function of spatial frequency, we can determine the effective diameter of the receptive-field center.

The laser beams overlapping on the retina will have a sinusoidal variation of electric-field strength and a sine-squared variation of intensity as a function of position on the retina. The maximum and minimum intensities that a given receptive field could measure as a function of spatial frequency may be computed as follows:

The light intensity on the retina is

$$I = I_1 + I_2 + 2\sqrt{I_1 I_2}\cos\left(\frac{2\pi d \sin\alpha}{\lambda}\right) \qquad (1)$$

For small α, $\sin\alpha \cong \alpha$;

and $I_1 = I_2$,

$$I = 2I_1\left[1 + \cos\left(\frac{2\pi d\alpha}{\lambda}\right)\right]$$

Using the relation $\cos 2x = 2\cos^2 x - 1$ and rearranging terms

$$I = 2I_1\left[2\cos^2\left(\frac{\pi d\alpha}{\lambda}\right)\right]$$

$$= 4I_1\cos^2\left(\frac{\pi d\alpha}{\lambda}\right)$$

Let $4I_1 = I_0$

$$w = \frac{\pi d}{\lambda D}$$

$x = \alpha D$ = distance on retina
D = distance between retina and nodal point of eye
d = separation of point sources in the pupil plane

$$\therefore I = I_0 \cos^2 (wx)$$

For intensity peak (I^+) at receptive field center,

$$I^+ = \int_0^{2\pi} \int_0^R I_0 \cos^2 (wx)\, r dr d\theta$$

Changing from polar to rectangular coordinates

$$I^+ = 2 \int_{-R}^{R} I_0 \cos^2 (wx) \sqrt{R^2-x^2}\, dx$$

where R = radius of receptive field center

For intensity minimum (I^-) at receptive field center

$$I^- = 2 \int_{-R}^{R} I_0 \sin^2 (wx) \sqrt{R^2-x^2}\, dx$$

The measured intensity contrast at a given spatial frequency is

$$C\ (R,w) = \frac{I^+ - I^-}{I^+ + I^-}$$

This response contrast, C, is plotted as a function of K = wR in Figure 4.

Light from the two separate point images of the laser source diverges from the nodal point of the eye. Since the point sources are coherent, interference occurs where their spherical wave fronts overlap. From equation (1), the angular separation of adjacent maxima in the retinal intensity distribution is

$$\theta = \frac{\lambda}{d}$$

where θ = angular separation of adjacent maxima in radians
λ = wavelength of laser source
d = separation of the point sources in the pupil plane

The linear separation of adjacent maxima, for small θ, is

$$y = \theta D$$

where y = distance between adjacent intensity maxima on retina in units of D
D = distance between nodal point and retina

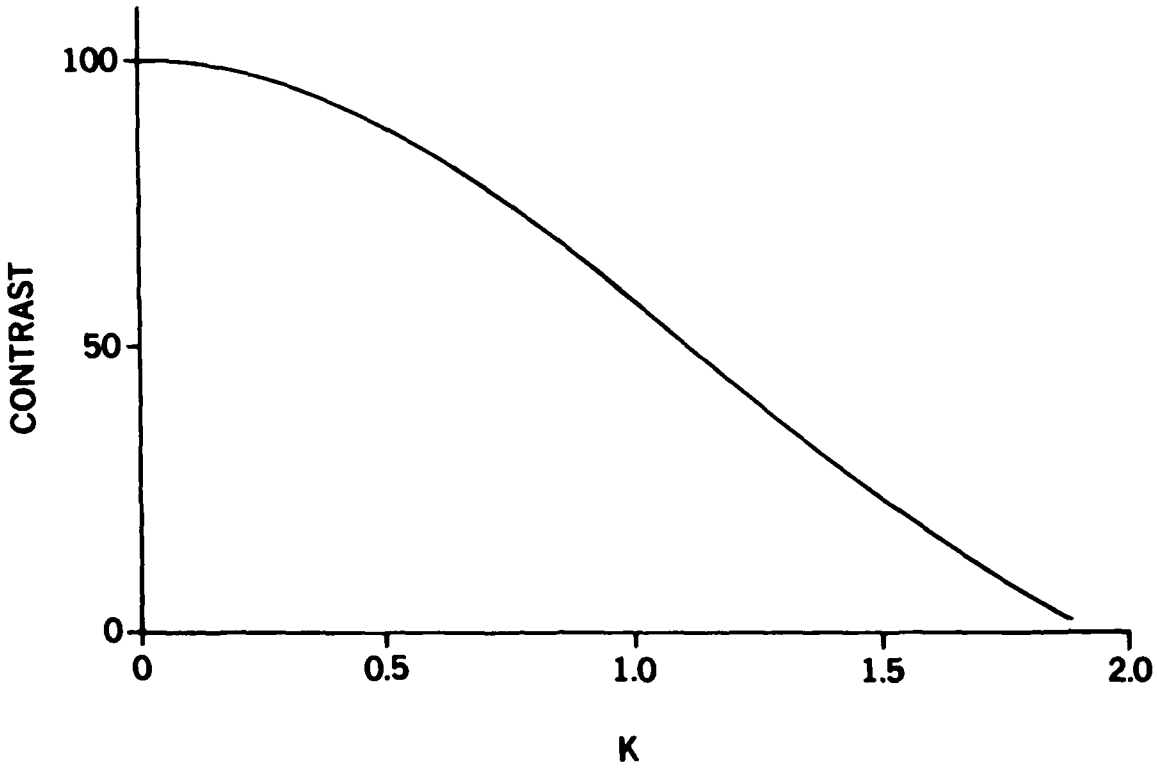

Figure 4. Contrast (%) of ganglion cell response vs K (K = wR). By measuring the contrast at a given spatial frequency, the effective receptive field radius can be determined from this plot.

The spatial frequency (f), i.e., the number of complete sinusoidal intensity cycles per unit distance along the retina, can be expressed as follows:

$$f = \frac{1}{y} = \frac{1}{\theta D} = \frac{1}{(\lambda/d)D}$$

$$\therefore f = \frac{d}{\lambda D}$$

Experimentally the effective radius, R, of a receptive field center can be determined by recording from a ganglion cell and measuring the response contrast as a function of spatial frequency. Using Figure 4, we have

$R = \frac{K}{w}$ for the effective radius of a receptive field center.

Now

$$R = \frac{K}{w} = \frac{K}{\pi d/\lambda D}$$

Again,

$$f = \frac{d}{\lambda D}$$

$$\therefore R = \frac{K}{\pi f}$$

For example, if a contrast of 50% (hence, K = 1.1) is measured at a spatial frequency of f = 0.35 cycles/μm (i.e., 86 cycles/degree of visual arc), then the effective radius of the receptive field center is 1 μm.

RESULTS

In these experiments, interference fringe patterns were moved across the receptive fields of 33 ganglion cells. Responses to more than one spatial frequency were recorded in only 12 of these cells. Of these 12 cells, only 5 are described in this paper. The data from the other cells were either recorded while the corneal drip system was functioning or were lost due to computer failure during the experiment.

Under the stimulus condition of drifting interference fringes, the luminance at each point of a cell's receptive field is modulated sinusoidally in time about some mean level. Because ganglion cell responses are the result of time-dependent processes occurring in the retina, the temporal characteristics of stimuli whose effects are to be compared must be the same. In other words, the temporal (drift) frequency of luminance changes should be kept constant. This is achieved for interference fringe patterns of different spatial frequencies drifting at constant velocity if the velocity is inversely proportional to the spatial frequency. In our experiments, the drift frequency was maintained at about 2.7 cycles/second. This frequency was chosen because it was in the approximate frequency region in which maximum response amplitude had been obtained (10) and because it was the highest frequency obtainable with our hydraulic microdrive system (limited at the lowest spatial frequency). Figure 5 shows the responses of a sustained on-cell to 530-nm interference fringes drifting across its receptive field; cell firing at the temporal drift frequency is periodically modulated. A shows the raw data histogram, and B the filtered histogram for comparison. Thirty sweeps in the same direction were averaged in the histogram. The contrast (0.70) of the response was one of the highest recorded.

One problem encountered early in the data collection was an artifactual low contrast of responses to the drifting interference fringes. The low contrast was caused by the corneal drip system. Figure 6 shows the response of a sustained on-cell to the fringes during the time the corneal drip system was functioning (A) and during the time it was off (B). The stimulus was the same in both cases, and the response in A was taken just before the one in B: it is evident that the corneal drip obscured the cell's response to the fringes. For subsequent experiments the corneal drip was turned off during data collection.

Figure 7 shows the responses of a sustained on-cell to 530-nm interference fringes of various spatial frequencies. Again, the cell firing rate is

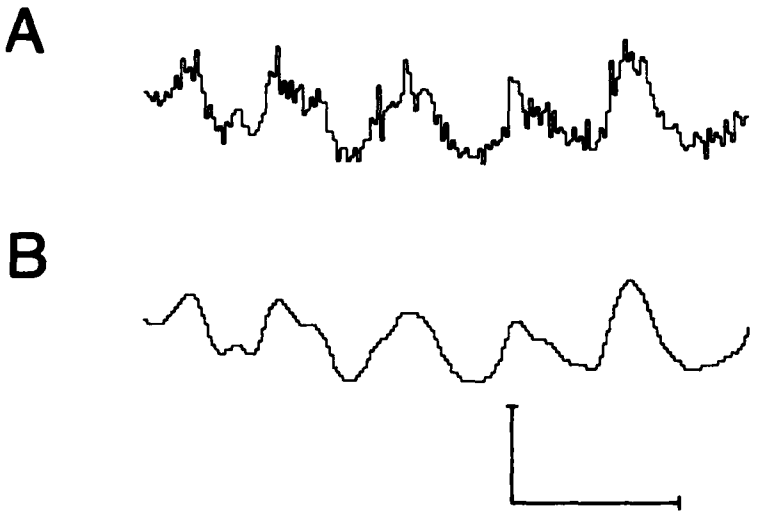

Figure 5. Unfiltered (A) and filtered (B) histograms of ganglion cell responses to drifting 530-nm interference fringes. Average of 30 sweeps in one direction. Drift frequency of 2.7 Hz, spatial frequency of 11.7 cycles/degree. Calibration bars: 40 impulses/sec, 500 msec.

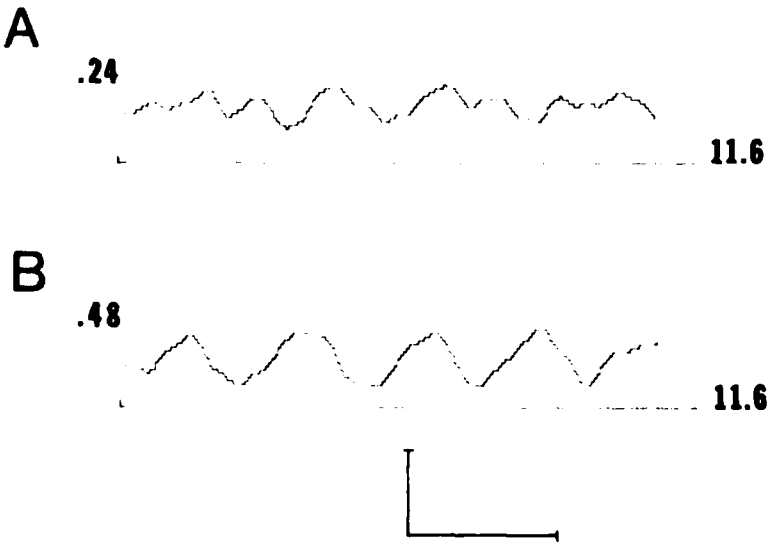

Figure 6. Effect of corneal drip on response histogram. A: Corneal drip (9 drops/min) was on during response averaging. B: Corneal drip was off for the 2 min of response averaging (1 min total for each direction). Average of 30 sweeps in one direction. Drift frequency of 2.7 Hz. Numbers at left are the rms contrasts of the response; numbers at right, the spatial frequencies of the interference fringes (cycles/degree). Calibration bars: 40 impulses/sec, 500 msec.

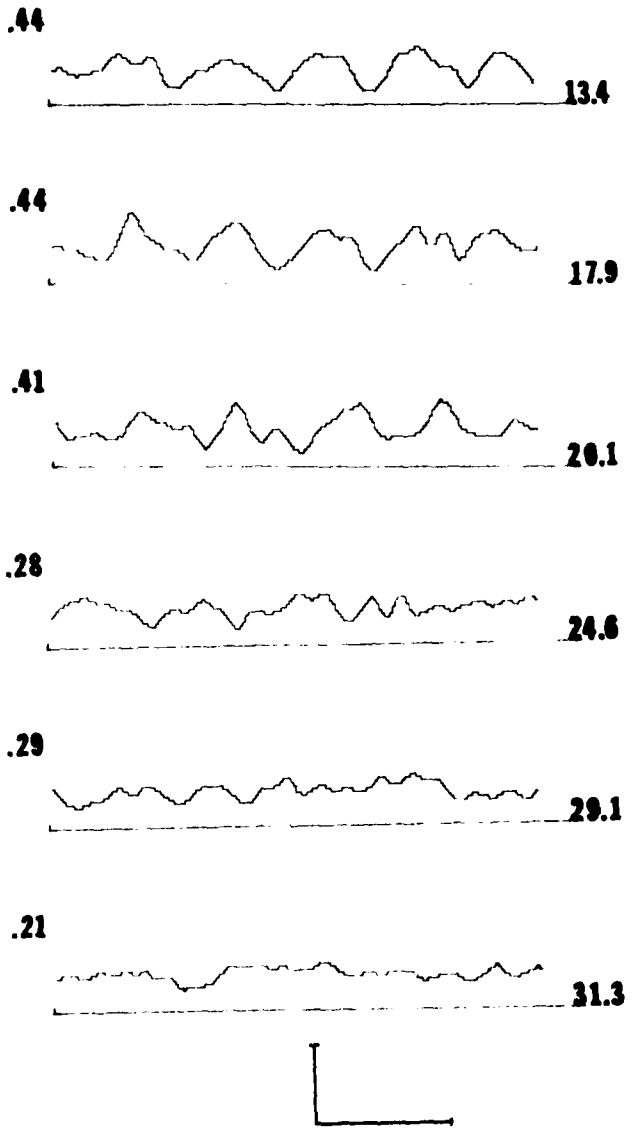

Figure 7. Responses of sustained, on-center ganglion cell to 530-nm interference fringes drifting in one direction of motion. No background illumination. Numbers at left are the rms contrast values; numbers at right, the spatial frequency of the interference fringes (cycles/degree). Calibration bars: 40 impulses/sec, 500 msec.

periodically modulated at the drift frequency. Also, the cell tends to modulate its responses around the same mean value (19.1±1.0 impulses/sec) at the various spatial frequencies. The contrast and the amplitude of the responses are clearly reduced at high spatial frequencies and apparently reach a plateau at the lowest spatial frequencies.

Figure 8 is a plot of the data from Figure 7 and an additional data point from the same cell. The additional data point is the contrast at 24.6 cycles/degree. Thus two contrasts were obtained at this spatial frequency, and they are in close agreement.

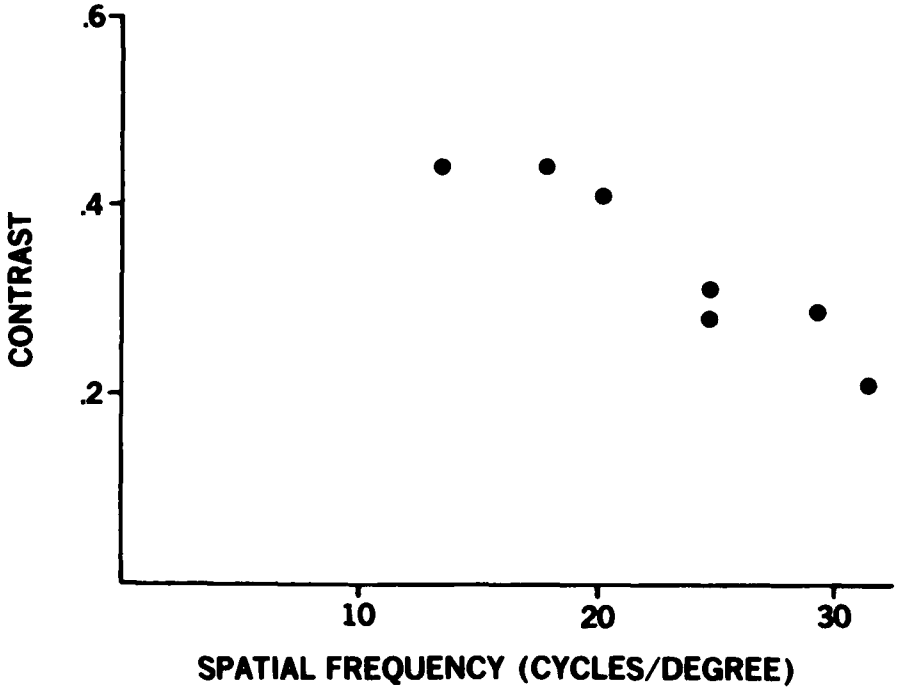

Figure 8. Contrast of responses of sustained, on-center ganglion cell of Fig. 7 vs spatial frequency of 530-nm interference fringes drifting across its RF center.

Figures 9-12 show the basic decrease in contrast with increasing spatial frequency for different cells, and they show the variability in the responses and contrast. Figures 9 and 10 show the responses of two sustained on-cells to drifting 530-nm interference fringes. The two middle histograms of Figure 9 are responses to the same spatial frequency.

Figures 11 and 12 show the responses of two color-opponent, sustained on-cells to drifting 530-nm interference fringes. Both of these cells had a green center/red surround. During the experiment constant red background illumination was used to adapt the surrounds out. Both figures show the initial decrease in contrast with spatial frequency and the variability of responses to fringe patterns.

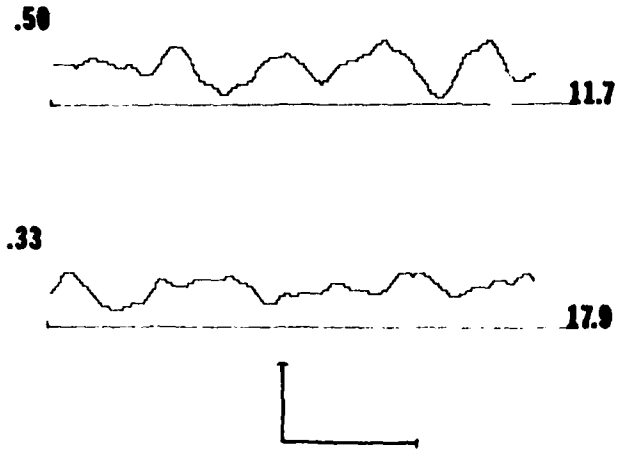

Figure 9. Responses of sustained, on-center cell to 530-nm interference fringes. No background illumination. (These responses are from a different monkey than those of Fig. 7.) Left corners: rms contrast; right: spatial frequency (cycles/degree). Calibration bars: 40 impulses/sec, 500 msec.

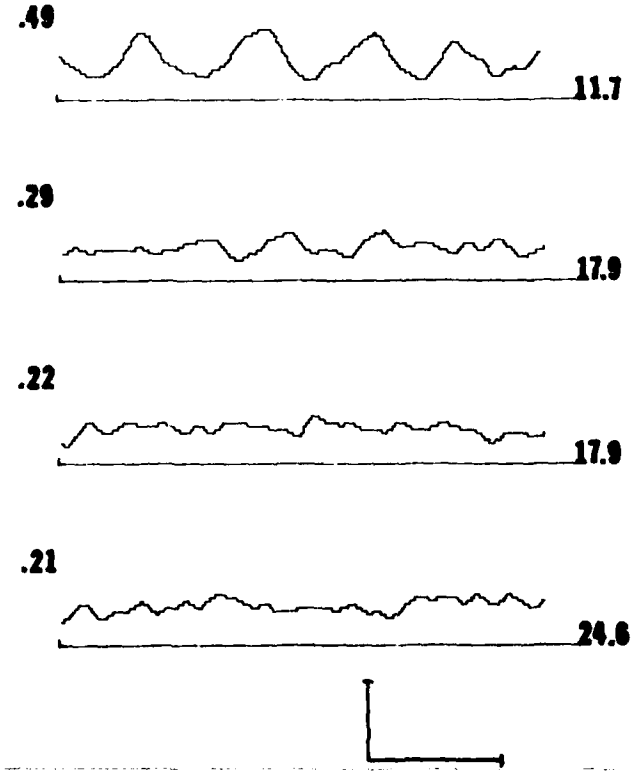

Figure 10. Responses of sustained, on-center cell to 530-nm interference fringes. No background illumination. (These responses are from a different cell than those in Fig. 9.) Left corners: rms contrast; right: spatial frequency. Calibration bars: 40 impulses/sec, 500 msec.

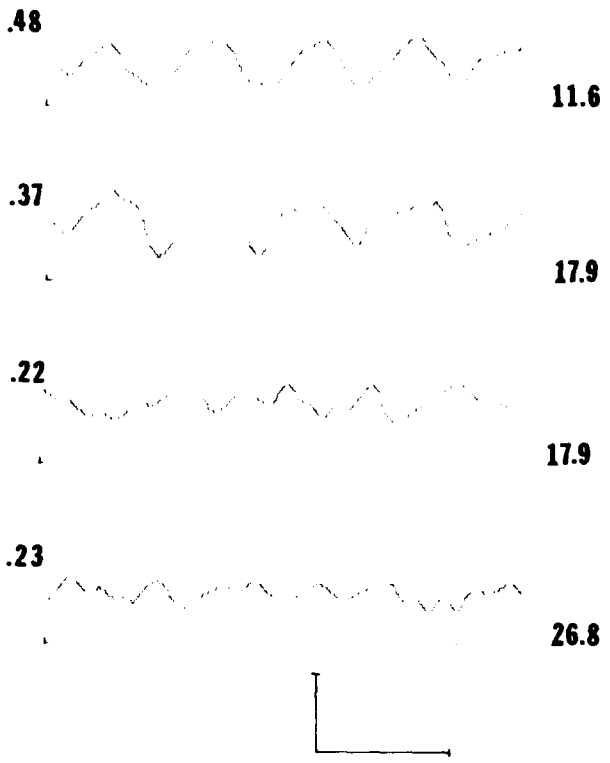

Figure 11. Responses of color-opponent (G/R), sustained on-center cell to 530-nm interference fringes with a red background. Left corners: rms contrast; right: spatial frequency. Calibration bars: 40 impulses/sec, 500 msec.

The middle histograms in Figure 11 are responses to the same spatial frequency (17.9 cycles/degree), yet their contrasts differ by a factor of 1.7. The first two histograms in Figure 12 are responses to the same spatial frequency (11.6 cycles/degree), yet their contrasts differ by a factor of 1.6. These disparities run contrary to the close agreement in Figure 8 of the contrasts at 24.6 cycles/degree.

The low contrasts (<0.25) observed for spatial frequencies above 17.9 cycles/degree may be within the noise level. As seen in Figures 7, 10, 11, and 12, the contrasts for spatial frequencies of 17.9 cycles/degree and above never go below 0.18. In Figures 10, 11, and 12 the contrast appears to fall quickly to the region between 0.18 to 0.25 and stay there as spatial frequency increases; however, the qualitative differences in this low-contrast region are remarkable. For example, the periodic modulation at the drift frequency can be seen in the lowest contrast (0.18) point in Figure 12 (spatial frequency of 22.4 cycles/degree). On the other hand, the modulation is not apparent at 31.3 cycles/degree in the same figure (contrast of 0.26) or at 24.6 cycles/degree in Figure 10 (contrast of 0.21). These differences probably reflect differences in RF size of the cell, as well as variability in the cell's response.

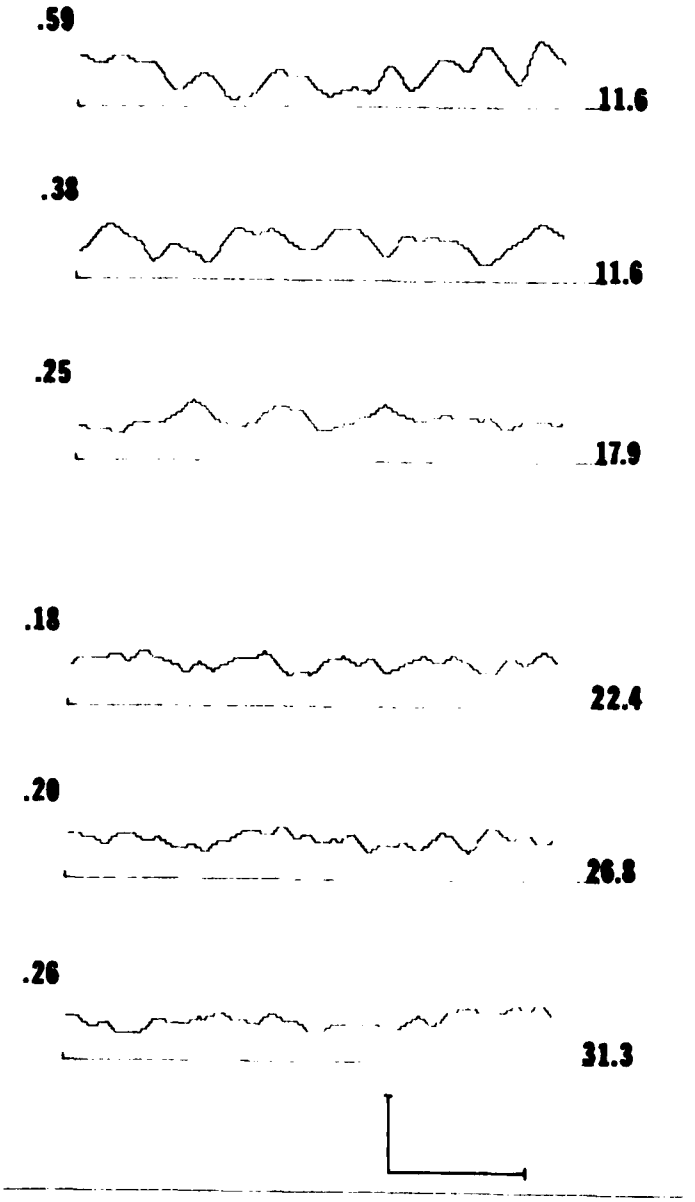

Figure 12. Responses of color-opponent (G/R), sustained on-center cell to 530-nm interference fringes with a red background. (These responses are from a different monkey than those in Fig. 10.) Left corners: rms contrast values; right: spatial frequency. Calibration bars: 40 impulses/sec, 500 msec.

Instead of using contrast as a measure of the response, some authors (11,12,16) have used the peak-to-peak amplitude (L_{max}-L_{min}). Figure 13 shows the data from Figures 7 and 11 replotted as (L_{max}-L_{min}) vs spatial frequency. Figure 14 shows the replotted data from Figures 9, 10, and 12. Both response measures, i.e., contrast and peak-to-peak amplitude, result in very similar plots. This reflects the fact that for each cell at the various spatial frequencies, the responses are modulated around the same mean spike frequency.

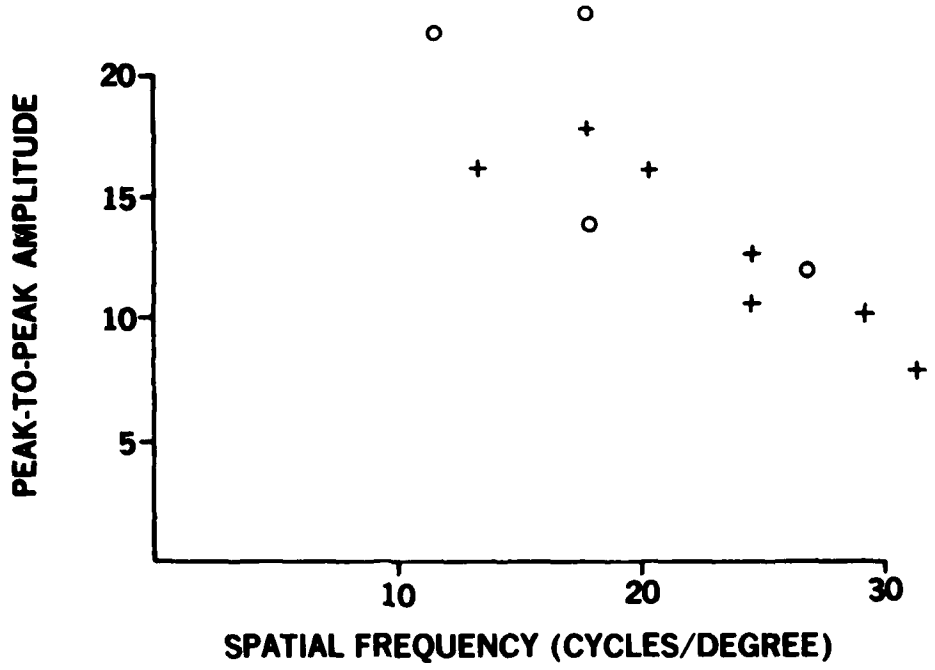

Figure 13. Data from cells in Figs. 7 (+) and 11 (•) replotted as peak-to-peak amplitude (L_{max}-L_{min} in spikes/sec) vs spatial frequency (cycles/degree).

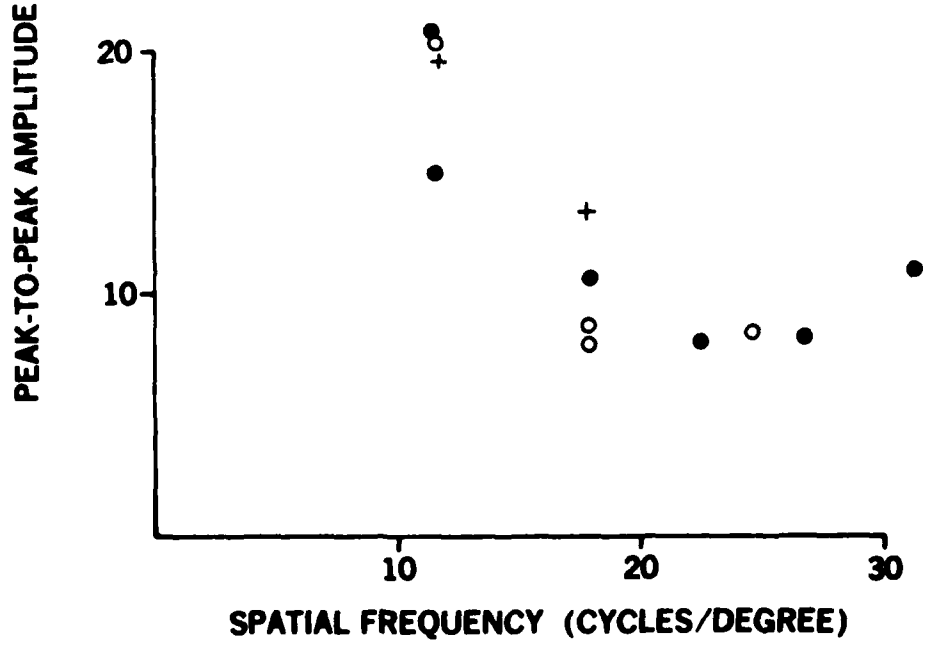

Figure 14. Data from cells in Figs. 9 (+), 10 (0), and 12 (•) replotted as peak-to-peak amplitude (L_{max} - L_{min} in spikes/sec) vs spatial frequency (cycles/degree).

DISCUSSION

When drifting interference fringes were used as a stimulus, the sustained on-cells in this study exhibited a periodic modulation of their firing rate around the same mean value for different spatial frequencies. This kind of response resembles the responses of X-cells in the rhesus (6) and in the cat (10) to drifting sinusoidal gratings focused on the retina. Responses to the grating in both animals were also modulated around the same mean value for different spatial frequencies. All of these responses reflect the linearity of the X-cell's spatial summation.

The results also show that the ganglion cell response magnitude (contrast) depends on the spatial frequency of the drifting interference fringes. The amplitude of the contrast was reduced at high spatial frequencies. One feature is of particular note. As the spatial frequency increased, the contrast of the response fell off more slowly with interference fringes than with sinusoidal gratings (6,10). Figure 15 shows the dependence of contrast on spatial frequency for sinusoidal gratings imaged on cat retina and rhesus retina, as well as two examples of our data for interference fringes. For the sinusoidal grating experiments, the contrast of the cat ganglion cell response was down to 0.5 at 1 cycle/degree and below 0.1 at 2 cycles/degree (10). The contrast of the rhesus ganglion cell response was down to almost 0.4 at 4 cycles/degree and down to almost 0.2 at 9 cycles/degree (6). So the responses to sinusoidal gratings were down to 0.2 or below before the spatial frequencies used in our experiments were reached.

At high spatial frequencies, rhesus ganglion cells respond better to interference fringes than to sinusoidal gratings. This phenomenon is easily explained by the fact that interference fringes on the retina are essentially independent of the optics of the eye while the sinusoidal gratings are not. In fact, the sinusoidal gratings were imaged by the eye's optics onto the retina. Hence, the reason for the different spatial frequency dependence is distortion due to the modulation transfer function of the eye's optics.

Our experiments have shown how the effective diameter of the center of a ganglion cell RF can be estimated. Figure 16 shows the contrast of the ganglion cell responses plotted as a function of the spatial frequency of the interference fringe patterns. The smooth curves in each plot show the theoretical model predictions for the indicated effective RF radius. These curves were fit by eye to the data for each cell. The effective RF radius was the adjustable parameter. The data are consistent with effective RF radii of from 3.4 to 5.0 μm, and hence with diameters of from 6.8 to 10 μm.

A simple calculation yields the possible number of cones corresponding to these effective RF centers. Cones in the rhesus macula are arranged in a tightly packed, hexagonal array (1,8,15). The most recent measurements of foveal cone densities and center-to-center distances were reported by Borwein et al. (2). Depending on location within the fovea, the cone densities range from 32,000 to 248,000 cones/mm^2, and the cone center-to-center distances range from 2 to 5 μm. Their data are consistent with the measurements of Polyak (15), Rolls and Cowey (19), Young (26), Boycott and Kolb (3), and Adams et al. (1). Assuming perfect hexagonal packing, their cone center-to-center distances imply cone densities of 30,800 to 192,000 cones/mm^2. The latter values were used in the following calculations.

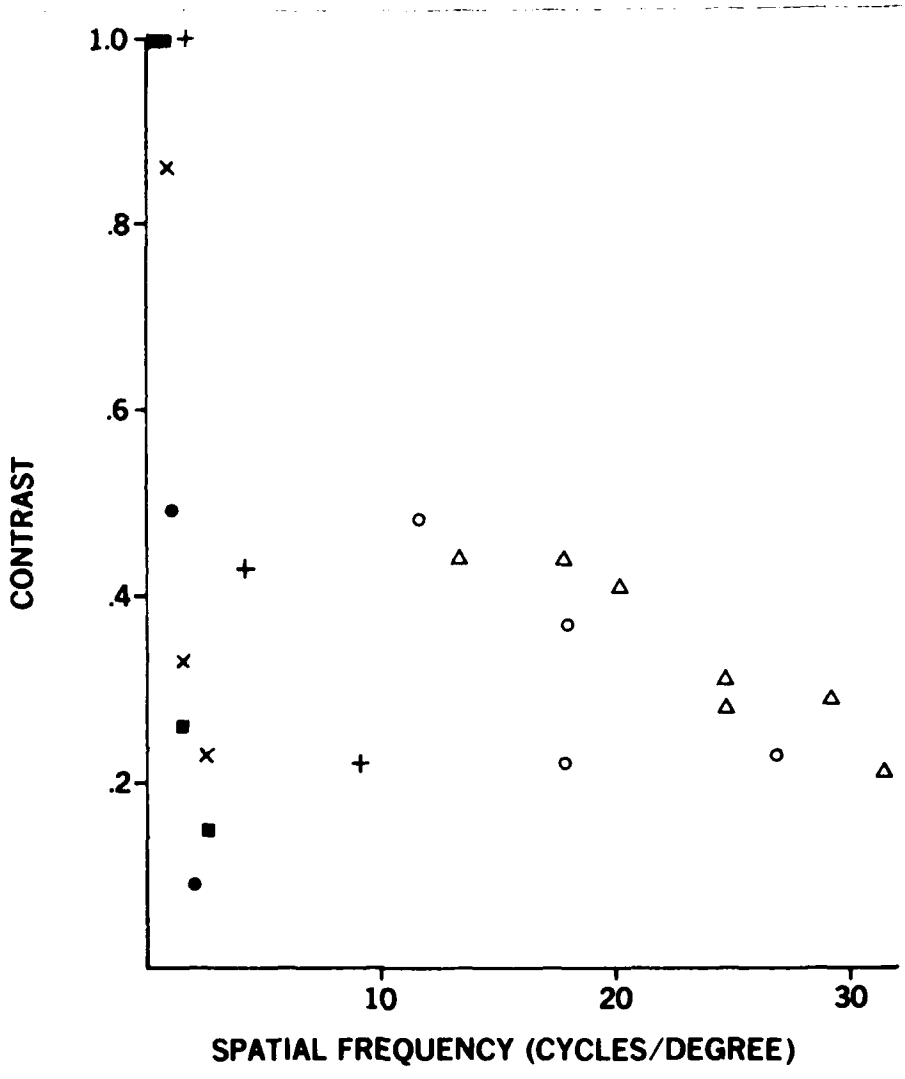

Figure 15. Contrast of ganglion cell responses vs spatial frequency from cat sinusoidal grating data (•) derived from Enroth-Cugell and Robson (10), from rhesus sinusoidal grating data (+, x, ■) derived from DeMonasterio (6), and from our interference fringe data in Figs. 7 (Δ) and 11 (o). All sinusoidal grating data fall below 10 cycles/degree; all interference fringe data fall above 10 cycles/degree.

By computing the area of the effective RF and multiplying by the extremes of cone density, the number or range of cones within the effective RF center can be estimated. Within the effective RF center with a 3.4-μm radius, there are 1-7 cones, depending on the cone density and therefore the position within the fovea. Within the effective RF center with a 5-μm radius, there are 2-15 cones, depending on density and position.

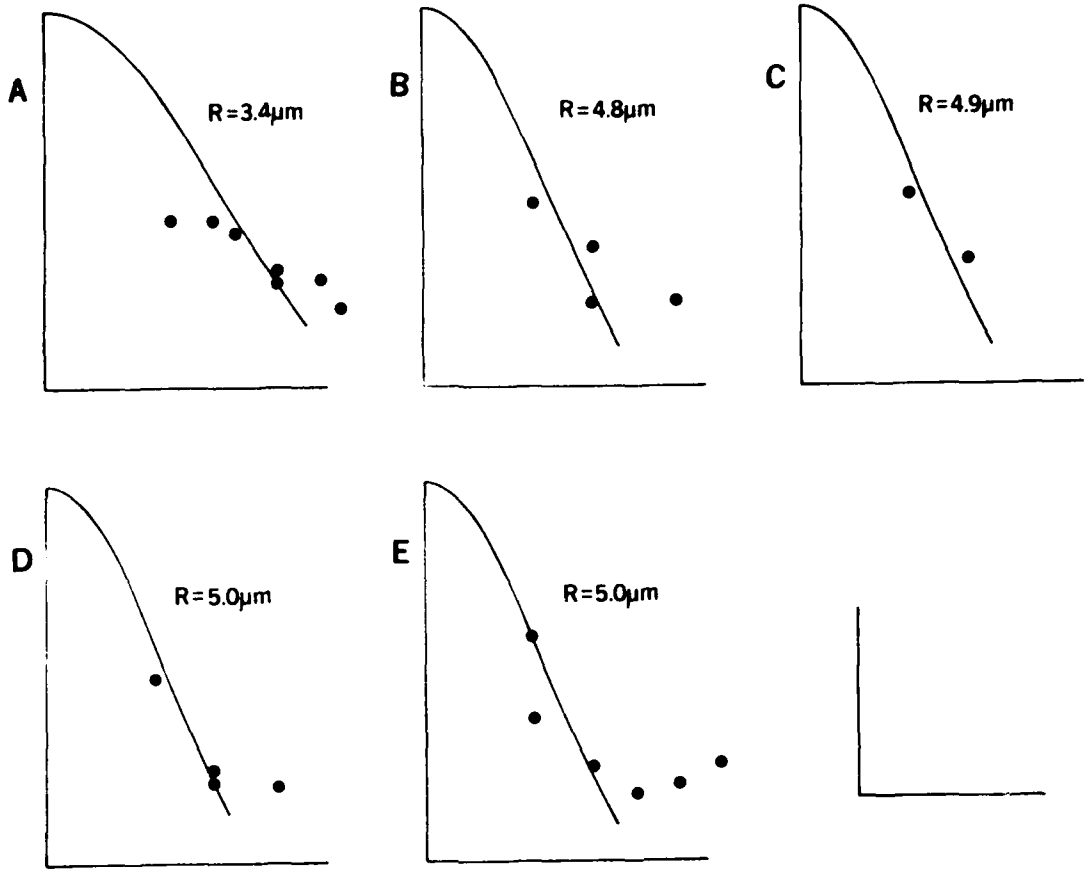

Figure 16. Contrast of ganglion cell responses vs spatial frequency. The smooth curves are the theoretical model predictions for the indicated effective RF radius (R). A--data from same cell as in Figs. 7 and 8; B--cell in Fig. 11; C--cell in Fig. 9; D--cell in Fig. 10; E--cell in Fig. 12. Calibration bars: 0.5 contrast, 20 cycles/degree.

These values for the number of cones within the RF center are maximum values because the estimation assumes that all cones within that area contribute to the ganglion cell response. However, for most color-opponent cells, the RF-center response is mediated by a single-color cone type, usually green or red cones (7). Any given area of retina will have a mixture of cone types; therefore, not all cones in that area will contribute to the ganglion cell response. To a first approximation in the foveal region, any given area will have equal numbers of green and red cones and essentially no blue cones. Hence, a revised estimate of the number of cones within the RF center is 1-3 cones in the 3.4-μm-radius RF and 1-7 cones in the 5-μm-radius RF center.

A number of experimental areas need to be extended and improved. One of the most important areas of needed improvement is the interference fringe generator. In the low spatial-frequency range, there are inherent difficulties in using the Ronchi-ruling technique to produce symmetrical interference fringes free of harmonics and irregularities (9). Hence, another technique for generating interference fringes should be used, perhaps the Moiré pattern technique (14) or the holographic phase grating technique (21).

Because of the physical aperture-size limitations in our equipment and the above-mentioned problems with the Ronchi-ruling approach, our setup could not achieve spatial frequencies below 10 or 11 cycles/degree. A significant extension of the data to lower spatial frequencies could be made by using a different technique for generating interference fringes.

Another improvement to the present studies would be to use a criterion response to measure contrast sensitivity. Signals from cone photoreceptors to X-ganglion cells are effectively linearly related to the incident illumination (6,10). Also, the incoming cone signals are linearly summed within the center and within the surround regions (6,10). However, it is the sensitivity of the ganglion cell, and not its response, that is linearly related to the stimulus magnitude (10). Therefore if the contrast required to evoke a criterion response from an X-cell is determined for various spatial frequencies, an estimate of the relative contrast sensitivity function can be obtained. In effect, this will yield the spatial contrast transfer function of the linear mechanisms.

ACKNOWLEDGEMENTS

I would like to thank Captain Garrett D. Polhamus for helpful discussions concerning the experimental setup. For their technical assistance, I would like to thank Mr. W. Rowe Elliott of Technology Incorporated, Staff Sergeant William D. Decker, Senior Airman Harvey M. Hodnett, Sergeant Robert Shepherd, Technical Sergeant John M. Turner, and Mr. Kennith W. Stevens.

REFERENCES

1. Adams, C. K., J. M. Perez, and M. N. Hawthorne. Rod and cone densities in the rhesus. Invest Ophthalmol Vis Sci 13:885-888 (1974).

2. Borwein, B., D. Borwein, J. Medeiros, and J. W. McGowan. Shape, dimensions, and structure of foveal cones of M. mulatta and M. irus. (Abstract) Invest Ophthalmol Vis Sci 18 (suppl.):79-80 (1979).

3. Boycott, B. B., and H. Kolb. The horizontal cells of the rhesus monkey retina. J Comp Neurol 148:115-140 (1973).

4. Campbell, F. W., and D. G. Green. Optical and retinal factors affecting visual resolution. J Physiol (Lond) 181:576-593 (1965).

5. Campbell, F. W., J. J. Kulikowski, and J. Levinson. The effect of orientation on the visual resolution of gratings. J Physiol (Lond) 187:427-436 (1966).

6. De Monasterio, F. M. Center and surround mechanisms of opponent-color X and Y ganglion cells of retina of macaques. J Neurophysiol 41:1418-1434 (1978).

7. De Monasterio, F. M., and P. Gouras. Functional properties of ganglion cells of the rhesus monkey retina. Physiol (Lond) 251:167-195 (1975).

8. De Monasterio, F. M., S. J. Schein, and E. P. McCrane. Staining of blue-sensitive cones of the macaque retina by a fluorescent dye. Science 213:1278-1281 (1981).

9. Enoch, J. M., and G. M. Hope. Interferometric resolution determinations in the fovea and parafovea. Doc Ophthalmol 34:143-156 (1973).

10. Enroth-Cugell, C., and J. G. Robson. The contrast sensitivity of retinal ganglion cells of the cat. J Physiol (Lond) 187:517-552 (1966).

11. Enroth-Cugell, C., T. K. Goldstick, and R. A. Linsenmeier. The contrast sensitivity of cat retinal ganglion cells at reduced oxygen tensions. J Physiol (Lond) 304:59-81 (1980).

12. Lee, B. B., A. Elepfandt, and V. Virsu. Phase of responses to moving sinusoidal gratings in cells of cat retina and lateral geniculate nucleus. J Neurophysiol 45:807-817 (1981).

13. Levick, W. R. Receptive fields of retinal ganglion cells, ch. 14, pp. 531-566. In M. G. F. Fuortes (ed.). Physiology of photoreceptor organs. Handbook of Sensory Physiology, Vol VII/2. New York: Springer-Verlag, 1972.

14. Lotmar, W. Use of Moiré fringes for testing visual acuity of the retina. Appl Optics 11:1266-1268 (1972).

15. Polyak, S. The vertebrate visual system. Chicago: University of Chicago Press, 1957.

16. Powers, M. K., and D. G. Green. Single retinal ganglion cell responses in the dark-reared rat: grating acuity, contrast sensitivity, and defocusing. Vision Res 18:1533-1539 (1978).

17. Rasmussen, K. E. Fixation in aldehydes: A study on the influence of the fixative, buffer, and osmolarity upon the fixation of the rat retina. J Ultrastruct Res 46:87-102 (1974).

18. Rodieck, R. W., et al. Residual eye movements in receptive-field studies of paralyzed cats. Vision Res 7:107-110 (1967).

19. Rolls, E. T., and A. Cowey. Topography of the retina and striate cortex and its relationship to visual acuity in rhesus monkeys and squirrel monkeys. Exp Brain Res 10:298-310 (1970).

20. Schiller, P. H., and J. G. Malpeli. Properties and tectal projections of monkey retinal ganglion cells. J Neurophysiol 40:428-445 (1977).

21. Smith, T. W., P. W. Remijan, W. Remijan, H. E. Kolder, and J. Snyder. A new test of visual acuity using a holographic phase grating and a laser. Arch Ophthalmol 97:752-754 (1979).

22. Westheimer, G. Modulation thresholds for sinusoidal light distributions on the retina. J Physiol (Lond) 152:67-74 (1960).

23. Wormington, C. M. In vivo measurement of the retinal point-spread function in the monkey eye. (In preparation)

24. Wormington, C. M., and H. A. Jaeger. A new microelectrode positioner for electrophysiology in the intact mammalian eye. (In preparation)

25. Wormington, C. M., and K. Stevens. A program for electrophysiological determination of point-spread function in intact mammalian eyes. (In preparation)

26. Young, R. W. The renewal of rod and cone outer segments in the rhesus monkey. J Cell Biol 49:303-318 (1971).


FILME
8